

Contents lists available at [ScienceDirect](http://www.sciencedirect.com)

Biochimica et Biophysica Acta

journal homepage: www.elsevier.com/locate/bbabio

Mitochondrial hyperpolarization during chronic complex I inhibition is sustained by low activity of complex II, III, IV and V

Marleen Forkink^a, Ganesh R. Manjeri^a, Dania C. Liemburg-Apers^a, Esther Nibbeling^a, Maxime Blanchard^b, Aleksandra Wojtala^c, Jan A.M. Smeitink^d, Mariusz R. Wieckowski^c, Peter H.G.M. Willems^a, Werner J.H. Koopman^{a,*}

^a Department of Biochemistry, Radboud Institute for Molecular Life Sciences, Radboud University Medical Centre, Nijmegen, The Netherlands

^b Department of Cell Physiology, Radboud Institute for Molecular Life Sciences, Radboud University Medical Centre, Nijmegen, The Netherlands

^c Nencki Institute of Experimental Biology, Warsaw, Poland

^d Department of Pediatrics, Nijmegen Centre for Mitochondrial Disorders, Radboud University Medical Centre, Nijmegen, The Netherlands

ARTICLE INFO

Article history:

Received 27 November 2013

Received in revised form 11 April 2014

Accepted 18 April 2014

Available online 24 April 2014

Keywords:

ATeam

Live-cell microscopy

Respirometry

TMRM

SypHer

ABSTRACT

The mitochondrial oxidative phosphorylation (OXPHOS) system consists of four electron transport chain (ETC) complexes (CI–CIV) and the F_0F_1 -ATP synthase (CV), which sustain ATP generation *via* chemiosmotic coupling. The latter requires an inward-directed proton-motive force (PMF) across the mitochondrial inner membrane (MIM) consisting of a proton (ΔpH) and electrical charge ($\Delta\psi$) gradient. CI actively participates in sustaining these gradients *via* trans-MIM proton pumping. Enigmatically, at the cellular level genetic or inhibitor-induced CI dysfunction has been associated with $\Delta\psi$ depolarization or hyperpolarization. The cellular mechanism of the latter is still incompletely understood. Here we demonstrate that chronic (24 h) CI inhibition in HEK293 cells induces a proton-based $\Delta\psi$ hyperpolarization in HEK293 cells without triggering reverse-mode action of CV or the adenine nucleotide translocase (ANT). Hyperpolarization was associated with low levels of CII-driven O_2 consumption and prevented by co-inhibition of CII, CIII or CIV activity. In contrast, chronic CIII inhibition triggered CV reverse-mode action and induced $\Delta\psi$ depolarization. CI- and CIII-inhibition similarly reduced free matrix ATP levels and increased the cell's dependence on extracellular glucose to maintain cytosolic free ATP. Our findings support a model in which $\Delta\psi$ hyperpolarization in CI-inhibited cells results from low activity of CII, CIII and CIV, combined with reduced forward action of CV and ANT.

© 2014 Elsevier B.V. All rights reserved.

1. Introduction

Mitochondria are double-membrane organelles involved in numerous cellular processes like apoptosis induction, reactive oxygen species generation, adaptive thermogenesis, ion homeostasis and innate immune responses [1]. Classically, mitochondria also act as key suppliers of cellular energy by providing the machinery that generates ATP from the energy stored in NADH and FADH₂. The latter two molecules are

generated by the glycolysis pathway in the cytosol (NADH) and the tricarboxylic acid (TCA) cycle in the mitochondria (NADH and FADH₂), and are oxidized at complex I (CI) and complex II (CII) of the electron transport chain (ETC), respectively. The released electrons are then transported to complex III (CIII) by coenzyme Q (CoQ) and subsequently to complex IV (CIV) by cytochrome c (cyt c). At the latter complex, the electrons react with molecular oxygen (O₂) to form water. Electron transport is energetically coupled to the translocation of protons from the mitochondrial matrix across the mitochondrial inner membrane (MIM) at CI, CIII and CIV. This results in an inward-directed proton-motive force (PMF) across the MIM that consists of a chemical (ΔpH) and an inside-negative electrical gradient ($\Delta\psi$).

Protons are allowed to flow back into the mitochondrial matrix *via* the F_0F_1 -ATP-synthase (CV) to drive the synthesis of ATP from ADP and inorganic phosphate (P_i). Together with CV, the four complexes of the ETC constitute the oxidative phosphorylation (OXPHOS) system. By reverse-mode action CV can also hydrolyse ATP and expel protons from the mitochondrial matrix thereby sustaining $\Delta\psi$ [2]. This mechanism requires that ATP is transported from the cytosol to the mitochondrial matrix by reverse-mode action of the mitochondrial adenosine

Abbreviations: ΔpH , pH gradient across the mitochondrial inner membrane; $\Delta\psi$, mitochondrial membrane potential; AA, antimycin A; ANT, adenine nucleotide translocase; BA, bongkrekic acid; CI–CV, complex I–complex V; CoQ, coenzyme Q; cyt c, cytochrome c; ETC, electron transport chain; FCCP, carbonyl cyanide-4-trifluoromethoxyphenyl-hydrazone; KCN, potassium cyanide; MALO, tert-butyl methyl malonate; MEFs, mouse embryonic fibroblasts; MIM, mitochondrial inner membrane; MOM, mitochondrial outer membrane; OLI, oligomycin A; OXPHOS, oxidative phosphorylation; PMF, proton motive force; PA, piericidin A; PM, plasma membrane; ROT, rotenone; RU, ratio units; TCA, tricarboxylic acid; TMRM, tetramethylrhodamine methyl ester

* Corresponding author at: 286 Biochemistry, Nijmegen Centre for Molecular Life Sciences, Radboud University Medical Centre, P.O. Box 9101, NL-6500 HB Nijmegen, The Netherlands. Tel.: +31 24 3614589; fax: +31 24 3616413.

E-mail address: w.koopman@ncmls.ru.nl (W.J.H. Koopman).

nucleotide translocase (ANT) or is generated by mitochondrial substrate-level phosphorylation [3].

A sufficiently large PMF is not only required to sustain ATP production but also is of crucial importance for mitochondrial fusion, protein import, metabolite exchange with the cytosol, and apoptosis induction (e.g. [4–8]). In this sense, $\Delta\psi$ can be considered as an important functional readout of mitochondrial health.

Mitochondrial dysfunction is a hallmark of (rare) metabolic disorders and also associated with normal human ageing, neurodegeneration, certain forms of cancer and metabolic syndrome [1,6–12]. Aberrations in $\Delta\psi$ have been observed in a wide variety of cells with inherited OXPHOS dysfunction. For instance cells with CV malfunction displayed $\Delta\psi$ hyperpolarization (i.e. the MIM was more inside-negative; [13,14]). In case of CI, we demonstrated that its partial enzymatic deficiency (i.e. residual CI activities between 18 and 75% of lowest controls) was associated with a minor decrease in $\Delta\psi$ (depolarization) in primary skin fibroblasts from patients with inherited CI deficiency [15,16]. Similarly, $\Delta\psi$ depolarization was observed in healthy primary skin fibroblasts when CI was partially and specifically inhibited by chronic treatment (72 h) with the CI inhibitor rotenone (ROT) [5,17]. In contrast, CI enzymatic deficiency was associated with $\Delta\psi$ hyperpolarization in immortalized mouse embryonic fibroblasts (MEFs) derived from whole-body knockout mice lacking the key CI subunit NDUFS4 [18]. Also in neurons, glial-like cells and their undifferentiated stem cells genetic CI dysfunction was accompanied by $\Delta\psi$ hyperpolarization [19]. Interestingly, whereas the $\Delta\psi$ of CI-deficient neurons seemed to be sustained by CV reverse-mode action, CV ran in forward mode in CI-deficient stem cells suggesting a cell type-specific regulation [19]. Compatible with these findings, specific CI inhibition (4 h) by a submaximal concentration of ROT induced $\Delta\psi$ hyperpolarization in 143B osteosarcoma cells [20]. However, in these cells $\Delta\psi$ depolarized when ROT was used at higher concentrations (>100 nM) and/or at longer incubation times. In contrast, $\Delta\psi$ hyperpolarization was induced when ROT was used at higher concentrations (i.e. >100 nM) but shorter incubation times (i.e. 30 min–2 h) in *Leishmania donovani* promastigotes [21], coronary artery smooth muscle cells [22] and neutrophils, but not in peripheral blood mononuclear leukocytes [23]. Taken together, it appears that CI functional impairment triggers $\Delta\psi$ hyperpolarization in a manner that (co)depends on the cell-type, inhibitor concentration and duration of inhibitor treatment.

This study aims to gain insight into the mechanism underlying $\Delta\psi$ hyperpolarization during chronic CI dysfunction. As a model system we used HEK293 cells in which $\Delta\psi$ hyperpolarization was triggered by chronic (24 h) incubation with the CI inhibitor ROT. Analysis of this model suggests that $\Delta\psi$ hyperpolarization during reduced CI activity requires low activity of CII, CIII and CIV in combination with greatly reduced forward activity of CV and the ANT.

2. Materials and methods

2.1. Generation of inducible HEK293 cell lines stably expressing cytosolic or mitochondria-targeted SypHer variants

Gateway® Entry vectors were generated by recombining Gateway-adapted PCR products containing the sequence encoding cyto-HyPer and mito-HyPer from pHyPer-cyto and pHyPer-dMito vectors (Evrogen, Moscow, Russia) with pDONR201 (Invitrogen, Breda, The Netherlands). A Gateway-adapted tag-less pcDNA/FRT/TO Destination vector was created by recombining the acGFP1-Destination vector [24–26] with a BacMamVSV-Destination vector [27]. To create constructs encoding the pH sensor SypHer, the mito-HyPer and cyto-HyPer Entry vectors were mutated at a critical cysteine residue by site-directed mutagenesis as described previously [28]. These new Entry vectors were recombined with the Gateway-adapted pcDNA/FRT/TO Destination vector to obtain mito-HyPer, mito-SypHer, cyto-HyPer and cyto-SypHer expression vectors. FLP-In T-REx293 cells (Invitrogen) were stably transfected

with the expression vectors described above using the SuperFect Transfection Reagent (Qiagen, Venlo, The Netherlands) and cultured for selection in the presence of 200 µg/ml hygromycin (Calbiochem, Brunschwig, Amsterdam, The Netherlands) and 50 µg/ml blasticidin (Invitrogen). To induce expression of the biosensor, 1 µg/ml doxycycline (Sigma-Aldrich, Zwijndrecht, The Netherlands) was added to the culture medium, followed by incubation for 24 h.

2.2. Generation of inducible HEK293 cell lines stably expressing cytosolic or mitochondria-targeted variants of ATeam 1.03 and “dead-ATeam”

The ATeam sequence was isolated from pcDNA3-AT1.03 and pcDNA3-mito-AT1.03 vectors [29], and selection markers and acGFP1 were removed from the acGFP1-Destination vector by digestion. The ATeam sequence was then ligated into the remaining Destination vector to obtain the pcDNA5/FRT/TO/cyto-ATeam and pcDNA5/FRT/TO/mito-ATeam expression vectors. FLP-In T-REx293 cells (Invitrogen) were stably transfected as described above. “Dead” ATeam was expressed in the cells using baculoviral transduction. To this end, the pcDNA3-AT1.03^{R122K/R126K} vector [29] was subcloned into cyto-ATeam and mito-ATeam Entry vectors using EcoRV and EcoRI to obtain a mutated ATP-unresponsive ATeam. Next, we recombined the Entry vectors with a Gateway-adapted BacMamVSV-Destination vector to obtain baculoviruses as described before [18]. FLP-In T-REx293 cells were seeded 48 h before imaging, and transfection was induced by the addition of 7% v/v baculovirus. The “dead” ATeam transfected cells were imaged and analyzed in the same way as the ATeam stable cell lines.

2.3. Cell culture and inhibitor treatment

FLP-In T-REx293 cells were cultured in DMEM containing 25 mM glucose, 2 mM L-glutamine, 10% (v/v) fetal calf serum and 1% penicillin/streptomycin in a humidified atmosphere containing 5% CO₂ at 37 °C. Prior to transfection, parental FLP-In TREx cells were cultured in the presence of 50 µg/ml blasticidin and 100 µg/ml Zeocin (Invitrogen). For fluorescence microscopy, 100,000 cells were seeded on 24-mm coverslips (Thermo Scientific, Etten-Leur, The Netherlands) placed in 35-mm CellStar tissue culture dishes (Sigma-Aldrich) or 35-mm glass-bottom culture dishes (Fluorodish, World Precision Instruments, Berlin, Germany) two days before imaging. For respirometry, the cells were grown to 80% confluence. One day after seeding, cells were treated with ROT, piericidin A (PA) or antimycin A (AA) for 24 h and compared with vehicle (0.1% ethanol)-treated (CT) cells.

2.4. High-resolution respirometry

Culture medium was collected, and cells were trypsinised, washed and resuspended to approximately one million cells/ml in the collected culture medium. Two ml of this suspension was used to measure cellular oxygen consumption. Oxygen consumption was measured at 37 °C using a two-chamber Oxygraph (Oroboros Instruments, Innsbruck, Austria) using an established protocol [30]. For inhibitor titration experiments, cells were allowed to respire for 10 min (routine respiration), after which ETC inhibitors were added in subsequent 1-µl volumes. As a control, identical additions were carried out using a vehicle (ethanol) solution.

For analyses in permeabilized cells, 1–1.5 million cells were resuspended in mitochondrial respiration medium [31] and, following baseline recording, CI-dependent respiration (10 mM glutamate, 2 mM malate, 1 mM ADP) was initiated by permeabilization with 2 µg/ml saponin. Then a maximum of 10 mM succinate was added (titration) to measure CI + CII, and respiration of CII substrates only was assessed by the addition of 100 nM ROT. Following determination of residual oxygen consumption using 2.5 µM AA, maximum CIV-dependent respiration was measured using 2 mM ascorbate and 0.5 mM TMPD. Finally,

the integrity of the mitochondrial outer membrane (MOM) was tested using 10 μ M cytochrome c.

2.5. Fluorescence imaging of free ATP levels

Free ATP levels were quantified using a fluorescence resonance energy transfer (FRET)-based reporter protein ('ATeam' 1.03). This sensor is comprised of the ϵ subunit of the bacterial F_0F_1 -ATP synthase sandwiched between cyan- and yellow-fluorescent protein variants [29]. The coverslips were washed with PBS, covered with HEPES-Tris (HT) buffer (containing 132 mM NaCl, 10 mM HEPES, 4.2 mM KCl, 1 mM $MgCl_2$, 1 mM $CaCl_2$ and 25 mM D-glucose, adjusted to pH 7.4 with Tris) and mounted in an incubation chamber that was placed on the temperature-controlled (37 °C) stage of an inverted microscope (Axiovert 200M, Carl Zeiss, Jena, Germany) equipped with a $\times 40$ 1.3 NA Fluor oil-immersion objective. The cyan fluorescent protein (CFP) of ATeam was excited at a wavelength of 430 nm, and the yellow fluorescent protein (YFP) was excited at 435 nm for 300 ms using a monochromator (Polychrome IV, TILL Photonics, Gräfelfing, Germany) and a 455DRLP dichroic mirror (Omega Optical Inc., Brattleboro, VT, USA). CFP and YFP emissions were directed through 480AF30 and 535AF26 (Omega) emission filters, respectively, and captured using a CoolSNAP HQ monochrome CCD camera (Roper Scientific, Évry, France). Microscopy hardware was controlled using MetaFluor 6.0 software (Universal Imaging Corporation, Downingtown, PA, USA). Ten fields of view were routinely analysed per coverslip. In time-lapse measurements a superfusion system [32] was used with a flow rate of 1.5 ml/min, and images were captured at an interval of 6 s. Images were analysed using MetaMorph 6.1 (Universal Imaging Corporation).

2.6. Fluorescence imaging of cytosolic and mitochondrial pH

Mitochondrial and cytosolic pH were measured in Flp-In T-Rex293 cells stably overexpressing the pH sensor SypHer. The latter was excited at 420 nm and 470 nm during 200 ms, directed by a 505DRLPXR (Omega) dichroic mirror. Emission signals were captured using a 535AF45 (Omega) emission filter using the microscopy system described above. Ten–fifteen fields of view were routinely analysed per coverslip.

2.7. Fluorescence imaging of mitochondrial membrane potential

Flp-In T-Rex293 cells were incubated with 50 nM of tetramethyl rhodamine methyl ester (TMRM; Invitrogen) in collected culture medium for 25 min at 37 °C and 5% CO_2 in the dark. The coverslips were then washed with PBS and imaged in HT buffer. Images were acquired on the microscope system described above using a 540-nm excitation wavelength directed for 100 ms by a 560DRLP (Omega) dichroic mirror through a 565ALP (Omega) emission filter. For each coverslip, 10–25 fields of view were routinely acquired and analysed using MetaMorph 6.1 (Universal Imaging Corporation). For time-lapse measurements, the images were recorded at 2-second intervals (carbonyl cyanide-4-trifluoromethoxyphenyl-hydrazone; FCCP) or 6-second intervals (oligomycin A; OLI or bongkrekic acid; BA).

2.8. Fluorescence imaging of mitoAcGFP1

Stable Flp-InT-REx293 cell lines expressing cox8-AcGFP1 [24] were excited at 488 nm for 300 ms, directed by a 505DRLPXR (Omega) dichroic mirror. Emission signals were captured using a 515ALP (Omega) emission filter using the microscopy system described above. Ten fields of view were routinely analysed per coverslip.

2.9. Immunocytochemistry

The cells were fixed using 4% formaldehyde in PBS for 15 min and permeabilized in 0.5% Triton X-100 in PBS for 20 min. After washing with 0.05% (v/v) Tween-20 in PBS, the cells were blocked in blocking buffer containing 2% (w/v) bovine serum albumin (BSA), 2% (v/v) normal goat serum (NGS), 0.1% (v/v) Triton X-100, 0.05% (v/v) Tween-20, and 100 mM glycine in PBS for 30 min. To determine tubulin morphology, the cells were incubated with the primary antibodies mouse anti-beta-tubulin (1:300, E7 IgG1). This antibody was developed by Michael Klymkowsky and obtained from the Developmental Studies Hybridoma Bank developed under the auspices of the NICHD and maintained by The University of Iowa, Department of Biological Sciences, Iowa City, IA 52242. Bound anti-beta-tubulin was visualized with AlexaFluor-488-labeled goat anti-mouse IgG1 (1:200; Molecular Probes). The cells were sealed using VECTASHIELD mounting medium containing 4',6-diamidino-2-phenylindole (DAPI), which stains all nuclei (Vector Laboratories, Burlingame, CA, USA) and visualized using a Zeiss AxioPhot2 fluorescence microscope with AxioCam MRm CCD camera.

2.10. Electrophysiology

Electrophysiological measurements of plasma membrane resting potential were performed using the perforated patch technique (50 μ M β -escin, Sigma-Aldrich) [33]. Data acquisition was performed using an EPC-9 amplifier and PatchMaster software (HEKA Electronics, Lambrecht, Germany). Pipettes were pulled from thin-walled borosilicate glass (Harvard Apparatus) and had resistance between 2 and 3 M Ω , when filled with pipette solution (120 mM KCl, 25 mM NaCl, 1 mM $CaCl_2$, 1 mM $MgCl_2$, 3.5 mM EGTA, 10 mM HEPES, adjusted to pH 7.3 using KOH). A perforated patch was generally obtained within 15 min following the establishment of the gigaseal. Plasma membrane resting potentials were obtained by injecting zero current in the current clamp-recording mode.

2.11. Data analysis and statistics

Curve fitting was performed using Origin Pro 6.1 (OriginLab Corp., Northampton, MA, USA). Additional image processing and analysis were carried out using Image Pro Plus 6.3 software (Media Cybernetics, Silver Spring, MD, USA). Unless stated otherwise, data is presented as mean \pm SE (standard error). Statistical significance was assessed using a Kruskal–Wallis 2-way ANOVA following Dunn's multiple comparison test, or a Mann–Whitney *t*-test using GraphPad Prism 5 software (GraphPad Software Inc., La Jolla, CA, USA). Asterisks indicate statistical significance: **P* < 0.05, ***P* < 0.01 and ****P* < 0.001.

3. Results

3.1. Acute rotenone treatment dose-dependently and incompletely inhibits O_2 consumption in intact cells

Triggered by experimental evidence in the literature (see Introduction) we first investigated whether it was possible to induce $\Delta\psi$ hyperpolarization in HEK293 cells by chronic treatment with the CI inhibitor ROT. However, when used at inappropriately high concentrations ROT can also display off-target effects on the cellular tubulin network. This might indirectly affect mitochondrial function (e.g. [5,20,34–37]). To avoid this potential problem we first determined the lowest ROT concentration that maximally inhibited cellular O_2 consumption when acutely added to intact cells (Fig. 1A). Up to a concentration of 1 μ M, ROT was unable to fully block respiration (i.e. down to the level of residual O_2 consumption; "ROX"). Similar results were obtained with the CI-specific inhibitor PA (Fig. 1A). Compatible with a previous binding study [38], PA displayed a somewhat lower IC_{50} than ROT. In contrast to ROT and PA, acute treatment with the CIII inhibitor AA (Fig. 1A) fully

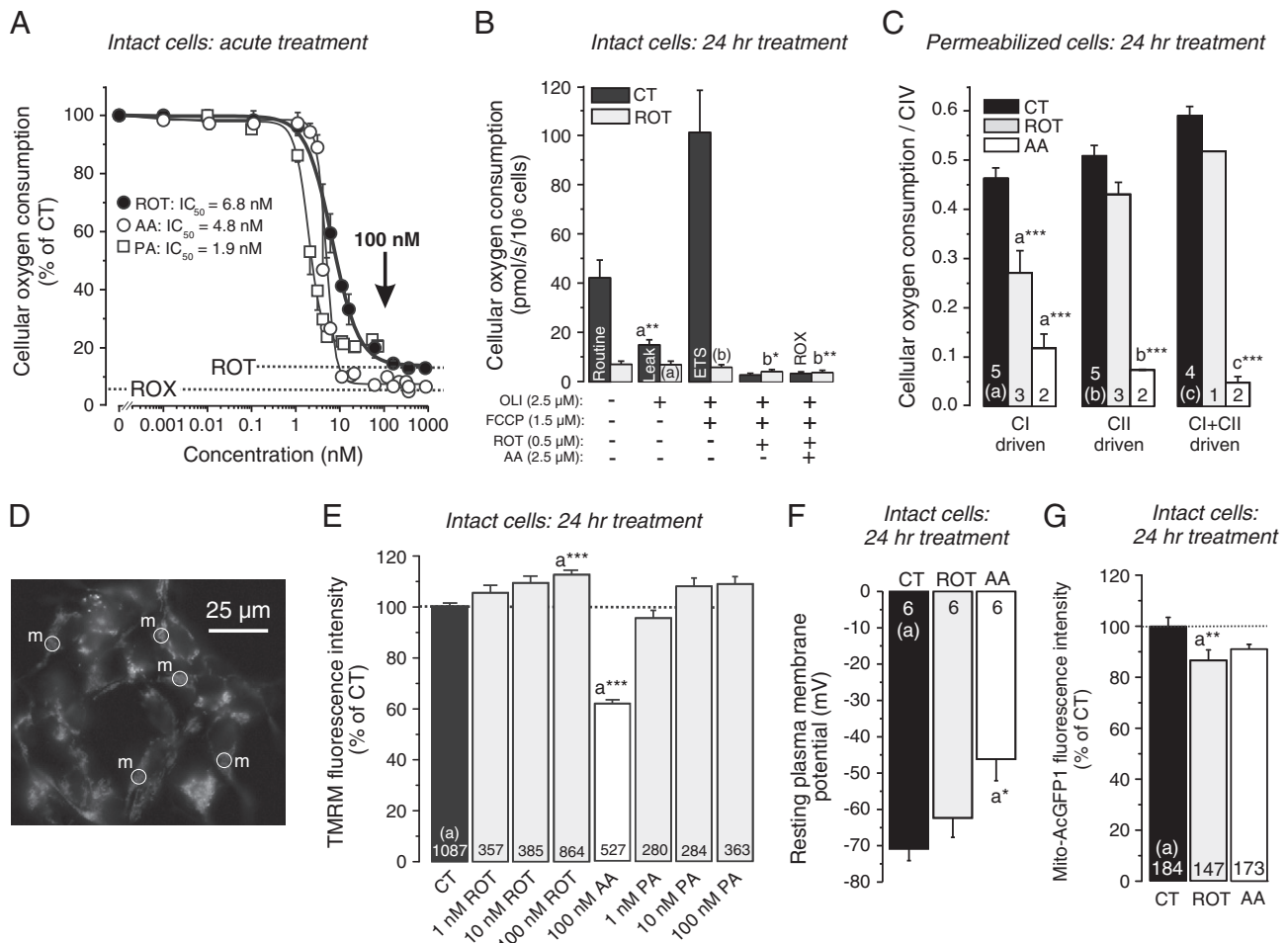


Fig. 1. Chronic complex I inhibition decreases cellular O_2 consumption and hyperpolarizes the mitochondrial membrane potential. (A) Stepwise inhibition of CI (ROT or PA) and CIII (AA) decreases the O_2 consumption of intact HEK293 cells in cell culture medium. Data points were fitted using a logistic model ($R^2 > 0.99$) to calculate IC_{50} values. Each data point reflects the mean of 4 (ROT) or 1–6 independent measurements (AA and PA). (B) O_2 consumption of CT and 100 nM ROT-treated (24 h) intact HEK293 cells in culture medium. Basal O_2 consumption ("Routine"), OLI-inhibited O_2 consumption ("Leak"), FCCP-induced maximal O_2 consumption (ETS) and ROT- and AA-induced residual O_2 consumption (ROX) are indicated. Each bar reflects the mean of 10 (CT) or 8 (ROT) independent experiments. Statistical significance was assessed using a Wilcoxon matched-pairs signed rank test. (C) CI (glutamate + malate and ADP), CI + CII (glutamate + malate + succinate and ADP) and CII-driven (+succinate and ROT) O_2 consumption in permeabilized HEK293 cells chronically treated (24 h) with vehicle (CT), 100 nM ROT or 100 nM AA (normalized on CIV-dependent respiration). O_2 consumption on CIV substrates (2 mM ascorbate and 0.5 mM TMPD) was similar for all conditions (not shown). (D) Typical example of TMRM-stained HEK293 CT cells and regions of interest ('m') for analysis of mitochondrial TMRM fluorescence intensity. (E) Effect of chronic treatment with ROT, PA or AA on mitochondrial TMRM fluorescence intensity. (F) The resting plasma membrane potential of inhibitor-treated (100 nM, 24 h) cells, measured by patch-clamping in two independent experiments. (G) Effect of chronic 100 nM ROT and AA treatment on mitochondrial GFP fluorescence intensity in mito-AcGFP1 expressing HEK293 cells after 24 h ($N = 2$). Statistics: * ($P < 0.05$), ** ($P < 0.01$), *** ($P < 0.001$), relative to the indicated columns (marked: a,b,c). Numerals indicate the number of individual experiments (panel C) or cells (panel E, F and G) analysed.

inhibited cellular O_2 consumption. Based upon these results, we decided to use a 100 nM ROT concentration during chronic cell treatment (24 h). Control experiments revealed that this treatment regime did not induce alterations in cell shape/size and organisation of the cellular tubulin network as detected with immunocytochemistry methods (data not shown).

3.2. Chronic rotenone treatment incompletely inhibits O_2 consumption in intact and permeabilized cells

Similar to acute ROT addition, chronic ROT treatment greatly reduced cellular O_2 consumption (Fig. 1B; grey bars vs. black bars). This O_2 consumption was insensitive to CV inhibition by OLI or mitochondrial uncoupling (FCCP). However, addition of ROT + AA slightly but significantly reduced O_2 consumption, suggesting that still some ETC activity remains in ROT-treated cells. To further dissect how chronic ROT treatment impacts on ETC-mediated O_2 consumption we analysed the effect of chronic ROT treatment in permeabilized cells (Fig. 1C; grey bars). Using CI- (glutamate + malate), CII-

(succinate + ROT) and CI + CII-selective (glutamate + malate + succinate) substrate conditions we observed that CI-dependent respiration was reduced (but not absent) and CII-dependent respiration was normal in ROT-treated cells. In contrast, cells chronically treated with AA (100 nM, 24 h) displayed greatly reduced O_2 consumption when respiring on CI or CII substrates.

3.3. Chronic rotenone treatment induces $\Delta\psi$ hyperpolarization and increases ΔpH

Chronic ROT treatment dose-dependently increased mitochondrial TMRM fluorescence compatible with a hyperpolarized (more negative) $\Delta\psi$ (Fig. 1D and E). Whereas a similar increase was observed in cells chronically treated with PA, chronic AA treatment reduced mitochondrial TMRM fluorescence (suggesting $\Delta\psi$ depolarization). Since the extent of mitochondrial TMRM accumulation also depends on the membrane potential of the plasma membrane (ΔV), it is of crucial importance to determine whether ROT treatment induces ΔV hyperpolarization [39]. Electrophysiological analysis revealed that chronic ROT

treatment did not significantly alter $\Delta\psi$ whereas AA induced a depolarization (Fig. 1F). These results argue against a mechanism where $\Delta\psi$ hyperpolarization in ROT-treated cells is caused by $\Delta\psi$ hyperpolarization. Since we used epifluorescence microscopy, and given the fact that TMRM is a single-excitation/single-emission reporter molecule, changes in mitochondrial and/or cellular volume and/or thickness can also affect TMRM fluorescence intensity. In this way, ROT-induced cellular and/or mitochondrial swelling might lead to an increased TMRM signal. We argued that if this would be the case, the emission intensity of another single-excitation/single-emission (but $\Delta\psi$ -independent) reporter molecule (i.e. a mitochondria-targeted GFP) should also be increased. However, ROT did not increase and AA did not significantly decrease the mitochondrial fluorescence signal of mito-AcGFP1 (Fig. 1G). This makes it highly unlikely that the ROT-induced increase in mitochondrial TMRM signal is due to cellular and/or mitochondrial swelling. Finally, to rule out interference of TMRM fluorescence autoquenching we performed time-lapse recordings to analyse the kinetics of the mitochondrial TMRM signal during protonophore (FCCP) application (Fig. 2A). Instead of a temporary increase in TMRM fluorescence (associated with autoquenching), FCCP induced a rapid fluorescence drop in vehicle (CT), ROT, AA and PA-treated cells (Fig. 2A). This demonstrates the

absence of TMRM autoquenching in our experiments. Taken together, our results support the conclusion that chronic CI inhibition induces $\Delta\psi$ hyperpolarization in HEK293 cells.

3.4. Chronic rotenone treatment does not induce matrix acidification

FCCP induced a faster mitochondrial TMRM release in CI-inhibited cells (Fig. 2B), suggesting that $\Delta\psi$ hyperpolarization is proton-dependent. To determine whether ROT treatment affected mitochondrial and cellular pH homeostasis we created two HEK293 cell lines stably expressing cytosolic and mitochondria-targeted variants of the pH-sensing protein “SypHer” (Fig. 2C), the fluorescence emission ratio of which increases as a function of pH [28]. Importantly, cyto- and mito-SypHer display identical pH-dependent changes in their emission ratio signal [28] allowing their quantitative comparison. In CT cells the pH within the mitochondrial matrix (pH_{mito}) was more alkaline than the pH in the cytosol (pH_{cyto} ; Fig. 2D) reflecting the presence of a matrix-directed PMF across the MIM. ROT treatment reduced pH_{cyto} but did not alter pH_{mito} , whereas AA treatment reduced both pH_{cyto} and pH_{mito} (Fig. 2E). We calculated the difference between the mitochondrial and cytosolic SypHer fluorescence for each condition and used this number

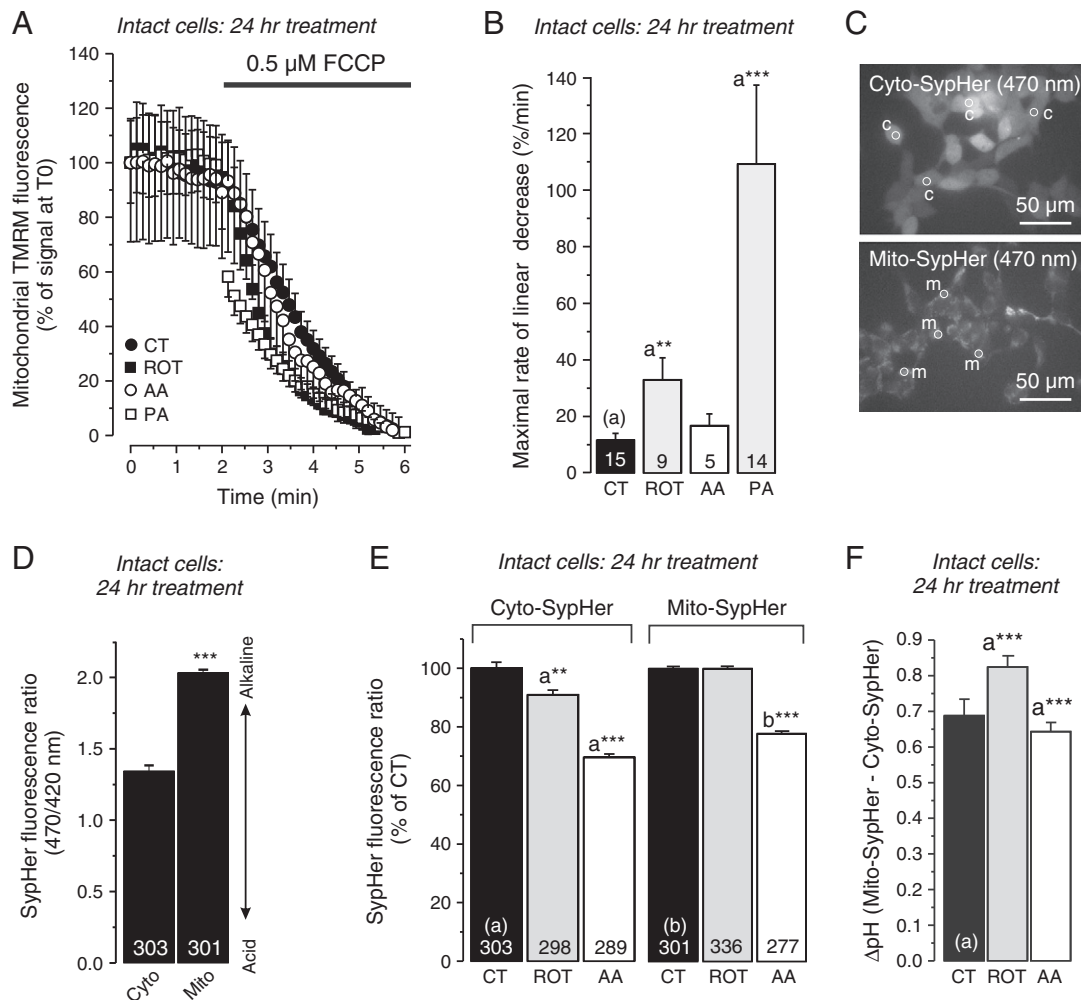


Fig. 2. Effect of chronic complex I and complex III inhibition on mitochondrial and cytosolic pH homeostasis. (A) Effect of acute addition of the uncoupler FCCP on the mitochondrial TMRM fluorescence intensity in cells treated with vehicle- (CT), 100 nM ROT, 100 nM AA or 100 nM PA for 24 h. (B) Rate of FCCP-induced decay determined using a linear fit to the curve (C) Typical images of CT cells expressing mitochondrial or cytosolic variants of the pH-sensing protein SypHer. (D) Steady-state fluorescence ratios of cells expressing Mito- or Cyto-SypHer. (E) Effect of 24 h 100 nM ROT or 100 nM AA treatment on the mito- and cyto-SypHer ratio. (F) Value of ΔpH , calculated by subtracting the cyto-SypHer from the mito-SypHer ratio presented in panel E. Statistics: * ($P < 0.05$), ** ($P < 0.01$), *** ($P < 0.001$), relative to the indicated columns (marked: a,b) or relative to the average value in the cytosol (“Cyto”; panel D). Numerals indicate the number of individual cells analysed.

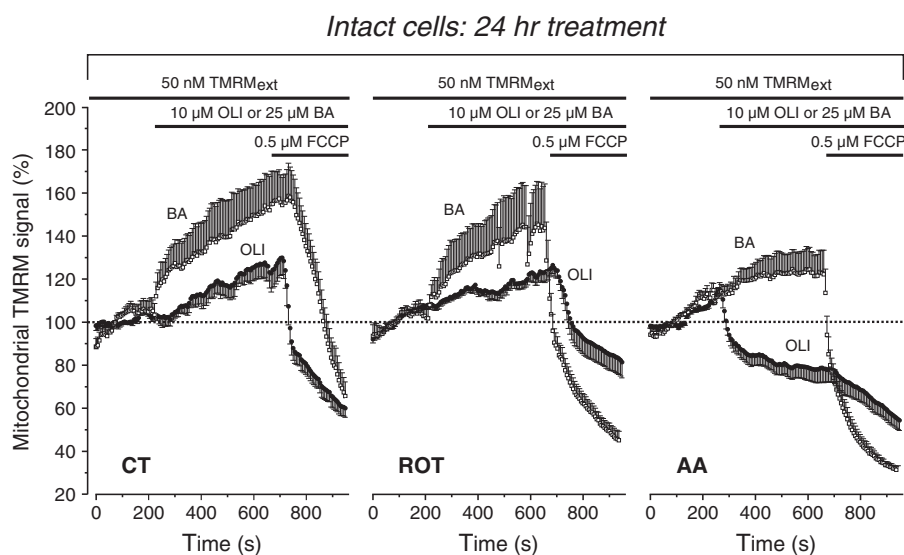


Fig. 3. Chronic CI inhibition does not induce CV reverse mode. Typical qualitative effects induced by acute application of the CV-inhibitor oligomycin (OLI, 10 μ M) or the ANT inhibitor bongkreic acid (BA, 25 μ M) on mitochondrial TMRM fluorescence in vehicle- (CT), ROT- or AA-treated cells (100 nM, 24 h). To facilitate visual inspection, the average pre-treatment signal was used for normalization and each curve is the average of 5–6 cells. Error bars reflect SEM.

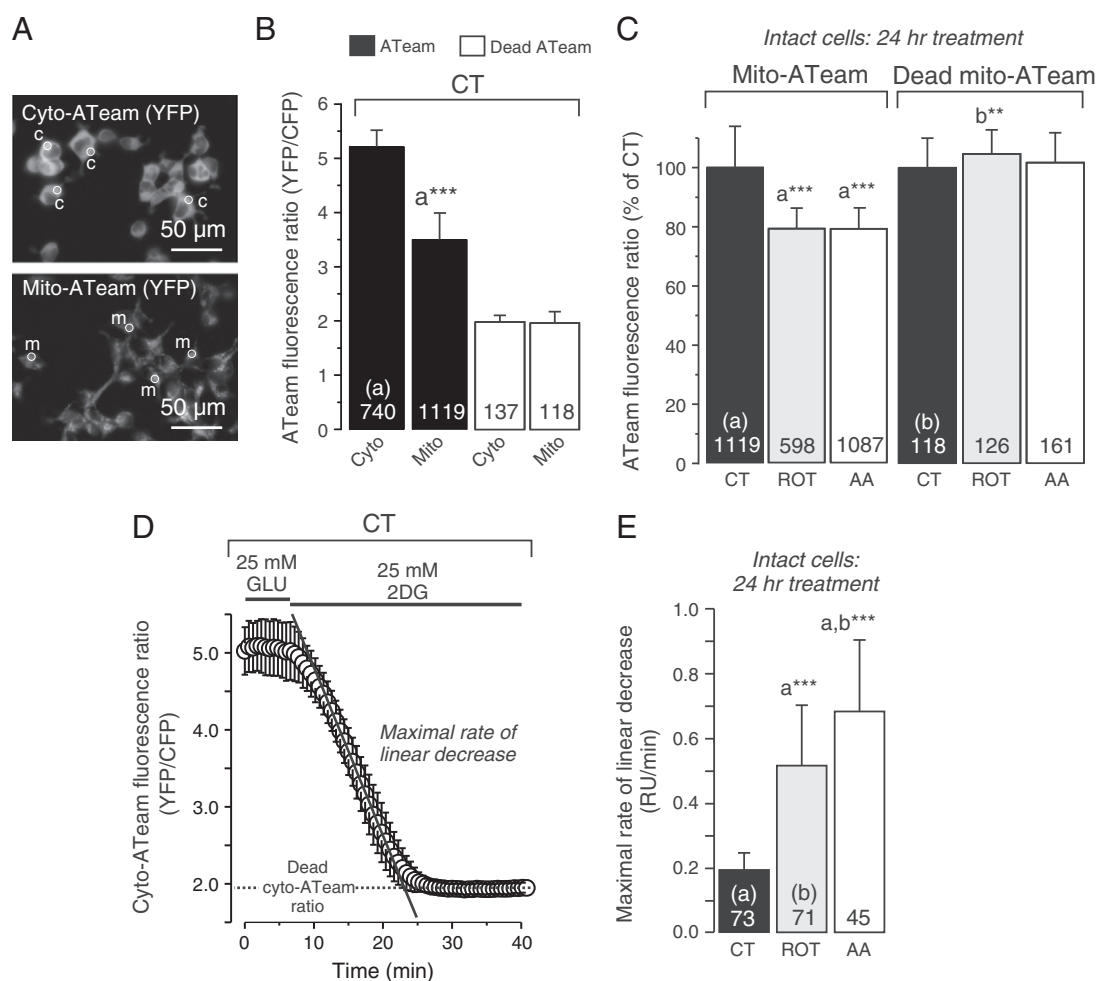


Fig. 4. Effect of chronic complex I and complex III inhibition on mitochondrial and cytosolic ATP homeostasis. (A) Typical images of CT cells expressing mitochondrial or cytosolic variants of the ATP-sensing protein “ATeam” (scale bar 50 μ m). (B) Steady-state fluorescence ratios of CT cells expressing Mito- or Cyto-ATeam and its ATP-insensitive variant “Dead ATeam”. (C) Effect of ROT or AA treatment on the fluorescence ratio signal of mito- and cyto-ATeam and dead ATeam. (D) Effect of replacement of extracellular glucose (GLU) by the glycolysis inhibitor 2DG, and vice versa, on the fluorescence ratio of cyto-ATeam. (E) Rate of decrease of the cyto-ATeam ratio upon replacement of GLU by 2DG as determined by a linear fit. (F) Rate of increase of the cyto-ATeam ratio upon replacement of 2DG by GLU as determined by a linear fit. Statistics: **($P < 0.01$), ***($P < 0.001$), relative to the indicated columns (marked: a,b). Numerals indicate the number of individual cells analysed. Error bars reflect SD.

as a semi-quantitative readout of the pH difference across the MIM (ΔpH). This difference was increased in ROT-treated cells and reduced in AA-treated cells (Fig. 2F), suggesting that the differential effects of these inhibitors on $\Delta\psi$ (partially) result from a change in trans-MIM proton gradient.

3.5. Chronic rotenone treatment does not induce reverse-mode action of complex V and the ANT

If ROT-induced $\Delta\psi$ hyperpolarization is primarily proton-based, it might result from an increased trans-MIM proton flux out of the matrix and/or a reduced trans-MIM proton influx into the matrix. Under conditions of ETC inhibition, $\Delta\psi$ hyperpolarization has been linked to reverse-mode action of CV and consumption of ATP [2,3,40]. When substrate-level phosphorylation cannot provide enough ATP to fuel CV reverse-mode action $\Delta\psi$ will further depolarize. To counterbalance this effect also the ANT can operate in reverse to bring in ATP and negative charge from the cytosol into the mitochondrial matrix [3]. Inhibition of CV (using OLI) or the ANT (using BA) did not induce $\Delta\psi$ depolarization in CT and ROT-treated cells (Fig. 3). BA similarly affected $\Delta\psi$ in AA-treated cells whereas OLI induced $\Delta\psi$ depolarization. Of note, in these experiments TMRM was also present outside the cell to allow for increased mitochondrial TMRM uptake during $\Delta\psi$ hyperpolarization. Qualitatively, these results suggest that: (i) CV and ANT operate in forward mode in CT cells, (ii) CV nor ANT reverse-mode action is involved in sustaining $\Delta\psi$ in ROT-treated cells, and (iii) CV operates in reverse-mode and ANT operates in forward mode in AA-treated cells.

3.6. Chronic rotenone treatment lowers mitochondrial free ATP levels

Above we provided evidence that ROT treatment greatly decreases cellular O_2 consumption and hyperpolarizes $\Delta\psi$, accompanied by an increase in ΔpH . Moreover, the differential effects of CV inhibition (OLI) on $\Delta\psi$ in ROT- and AA-treated cells (Fig. 3) suggest that also steady-state mitochondrial ATP levels, which depend on the balance between ATP production, ATP consumption and ANT-mediated exchange, might be differentially affected. In CT cells, CV inhibition decreases cellular respiration by >70%, indicating that these cells contain an active mitochondrial ATP production supported by CV forward operation (Fig. 1B; black bars). CV inhibition did not depolarize but, in contrast to CT cells, also did not greatly hyperpolarize $\Delta\psi$ in ROT-treated cells. This suggests that CV activity is reduced in ROT-treated cells. Therefore it appears that in ROT-treated cells the driving force of the PMF is uncoupled from CV-mediated ATP production. To address this hypothesis we generated two HEK293 cell lines stably expressing cytosolic and mitochondria-targeted variants of the ATP-sensing protein “ATeam” (Fig. 4A), the fluorescence emission ratio of which increases as a function of free ATP concentration [29]. As controls, we expressed cytosolic and mitochondria-targeted variants of an ATP-insensitive ATeam variant (“dead ATeam” [29]) using a baculoviral expression system. In CT cells the fluorescence emission ratio of mito-ATeam was lower than that of cyto-ATeam (Fig. 4B; black bars), whereas these ratios were lower but identical for dead mito-ATeam and dead cyto-ATeam (white bars). This demonstrates that both cyto- and mito-ATeam variants bind ATP and that $[\text{ATP}]_m$ is lower than $[\text{ATP}]_c$ in HEK293 cells. The mito-ATeam emission ratio was reduced in ROT- and AA-treated cells (Fig. 4C; left panel). These treatments did not decrease the emission ratio of dead mito-ATeam (Fig. 4C; right panel). Taken together, this demonstrates that $[\text{ATP}]_m$ is reduced in ROT- and AA-treated cells. Although ROT- and AA-treatment did not alter the emission ratio of cyto-ATeam (data not shown), suggesting that $[\text{ATP}]_c$ is not affected, we did not use this data since $[\text{ATP}]_c$ might be far above the ATP affinity of this sensor [41]. However, when glucose (GLU) in the extracellular medium was replaced by an equimolar amount of the competitive hexokinase inhibitor 2-Deoxy-D-Glucose (2DG) the cyto-ATeam ratio

in CT cells dropped within 15 min to that of dead cyto-ATeam (Fig. 4D). This means that cytosolic ATP was fully depleted within this time period. Upon 2-DG application $[\text{ATP}]_c$ decreased much faster in ROT- and AA-treated cells than in CT cells (Fig. 4E). These results, in combination with the observed low O_2 consumption values, demonstrate that inhibitor-treated cells are more glycolysis-dependent than CT cells for maintaining their $[\text{ATP}]_c$. Taken together, these data suggest that CV is less involved in residual mitochondrial ATP production in CI-inhibited cells, despite the presence of a substantial PMF.

3.7. Chronic inhibition of complex II, III or IV prevents rotenone-induced $\Delta\psi$ hyperpolarization

The above results argue against involvement of CV and ANT reverse-mode action in ROT-induced $\Delta\psi$ hyperpolarization. Moreover, because $[\text{ATP}]_m$ is decreased and oxygen consumption is reduced, it seems that CV is less active in CI-inhibited cells. This hypothesis is supported by our result that $\Delta\psi$ was most sensitive to FCCP-induced proton leak in ROT- or PA-treated cells (Fig. 2B). This suggests that activity of other ETC complexes (CII, CIII and CIV) is required to allow ROT-induced $\Delta\psi$ hyperpolarization. Chronic inhibition of CII (MALO), CIII (AA) or CIV (KCN) resulted in reduced mitochondrial TMRM fluorescence compatible with $\Delta\psi$ depolarization (Fig. 5). For the purpose of comparison, we have included the data for 100 nM ROT and AA from Fig. 1E in Fig. 5. Interestingly, ROT-induced $\Delta\psi$ hyperpolarization was prevented by chronic co-inhibition of CII (ROT + MALO), CIII (ROT + AA) or CIV (ROT + KCN) (Fig. 5), suggesting that activity of these complexes plays an essential role in the hyperpolarization mechanism.

Inhibition of CII alone and CI + CII reduced mitochondrial TMRM fluorescence to a similar extent, whereas inhibition of CI + CIII and CI + CIV was less efficient (Fig. 5). Since in ROT-treated cells CII-driven respiration is unchanged compared to CT (Fig. 1C) but respiration on endogenous substrates is low (Fig. 1B), it seems that CII activity drives a low level of electron transport in ROT-treated cells. Therefore we conclude that CII plays a key role in sustaining $\Delta\psi$

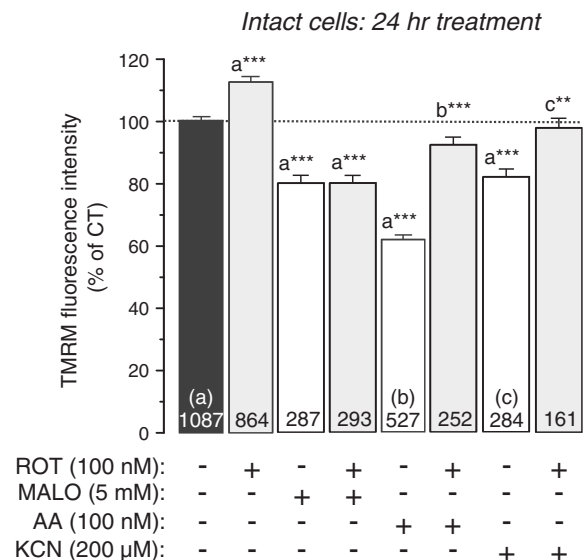


Fig. 5. The involvement of other ETC complexes in CI inhibition-induced mitochondrial hyperpolarization. Effect of co-inhibition of CII (using MALO), CIII (AA) or CIV (using KCN) on mitochondrial TMRM fluorescence intensity in ROT-treated HEK293 cells (24 h treatments). For visualization purposes, data for 100 nM ROT (bar 2) and 100 nM AA (bar 5) from Fig. 1E were also included. Statistics: **($P < 0.01$), ***($P < 0.001$), relative to the indicated columns (marked: a,b,c). Numerals indicate the number of individual cells analysed.

hyperpolarization in ROT-treated cells by fuelling electron transport to CIII and CIV.

4. Discussion

Chemical or mutation-induced inhibition of the mitochondrial ETC reduces proton efflux across the MIM and is generally associated with (partial) $\Delta\psi$ depolarization [5,42]. However, various (patho)physiological conditions including mitochondrial CI deficiency have been linked to $\Delta\psi$ hyperpolarization [18–23], the mechanism of which is incompletely understood. Here we demonstrate that chronic (24 h) treatment with the mitochondrial CI inhibitor ROT induces $\Delta\psi$ hyperpolarization in HEK293 cells. This model system was used to study the mechanism of mitochondrial hyperpolarization during chronic CI dysfunction.

Acute treatment of HEK293 cells with the CI inhibitors ROT or PA dose-dependently but not completely inhibited cellular O_2 consumption. In contrast, inhibition of CIII using AA fully blocked cellular O_2 consumption. Following chronic ROT treatment (100 nM; 24 h), cells still displayed ROT and/or AA-sensitive respiration, suggesting that also after this time period cellular O_2 consumption was not fully inhibited. Using this chronic treatment regime, we did not observe off-target effects of ROT on cell shape/size and organisation of the cellular tubulin network. Analysis of permeabilized cells revealed that ROT- and AA-treated cells displayed lower O_2 consumption when respiring on CI-selective substrates. In contrast, ROT-treated cells exhibited normal O_2 consumption when respiring on CI + CII- or CII-selective substrates whereas these parameters were greatly reduced in AA-treated cells. These results suggest that the greatly reduced O_2 consumption in

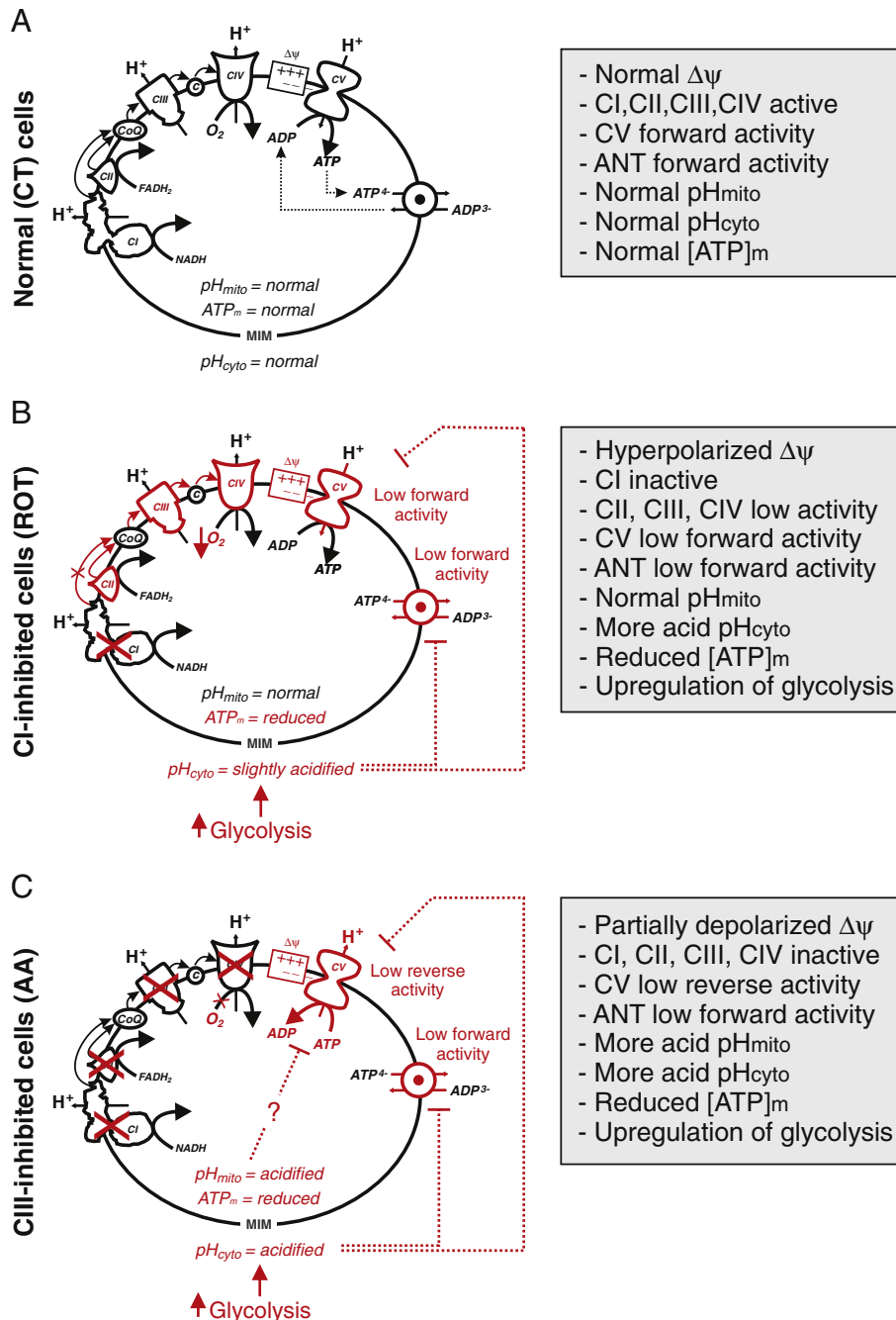


Fig. 6. Proposed mechanism for $\Delta\psi$ hyperpolarization and depolarization in HEK293 cells during chronic complex I or complex III inhibition. For details, see Discussion.

ROT-treated cells is primarily driven by CII-mediated substrate oxidation and subsequent electron transport to CIII and CIV. However, we cannot rule out that a low remaining CI activity co-contributes to residual ROT-sensitive O_2 consumption in the ROT-treated cells. In case of AA, its full inhibition of O_2 consumption is compatible with the very low rates on CI, CII and CI + CII-selective substrates.

Single cell microscopy analysis was used to quantify accumulation of the $\Delta\psi$ -dependent fluorescent cation TMRM within the mitochondrial matrix. It was found that chronic ROT and PA treatment dose-dependently increased the mitochondrial TMRM fluorescence signal. Chronic treatment with 100 nM AA, a concentration that fully blocked cellular O_2 consumption, induced a decrease in this signal. Importantly, the intensity of the mitochondrial TMRM fluorescence not only depends on $\Delta\psi$ but also can be affected by the potential of the plasma membrane (ΔV), changes in mitochondrial and/or cellular volume and/or thickness, and TMRM autoquenching. However, control experiments revealed that these “artifacts” were not responsible for the observed ROT-induced $\Delta\psi$ hyperpolarization. In case of AA treatment a significant ΔV depolarization was observed suggesting that the reduced TMRM accumulation under these conditions might be overestimated. In the light of the above, we conclude that the ROT-induced increase in mitochondrial TMRM accumulation truly reflects $\Delta\psi$ hyperpolarization that is associated with CI inhibition. It appears that this hyperpolarization is CI-specific, since it was dose-dependently increased by ROT or PA and not induced by chronic inhibition of the other ETC complexes. When cells were cultured in the chronic presence of ROT + AA, ROT + MALO or ROT + KCN, no $\Delta\psi$ hyperpolarization was observed. This strongly suggests that $\Delta\psi$ hyperpolarization in ROT-treated cells requires activity of these complexes, supporting our above conclusion that CII-mediated substrate oxidation and electron transport to CIII and CIV sustains the greatly reduced O_2 consumption in these cells. However, we cannot exclude the presence of CoQ-mediated electron entry via other enzymes like the electron-transferring flavoprotein (ETF)-ubiquinone oxidoreductase, *s,n*-glycerophosphate dehydrogenase and dihydroorotate dehydrogenase (see Ref. [5] and the references therein). ROT- and PA-inhibited cells were particularly sensitive to chemical uncoupling by FCCP. This demonstrates that $\Delta\psi$ is (partially) carried by protons under these conditions and primed us to quantify mitochondrial and cellular pH using the protein-based sensor SypHer. The SypHer analysis demonstrated that $pH_{mito} > pH_{cyto}$, indicative of an inward directed trans-MIM proton gradient, allowing forward-mode (*i.e.* ATP producing) action of CV. The latter is compatible with our observation that CT cells displayed an OLI-sensitive O_2 consumption meaning that their mitochondria were actively producing ATP. Whereas chronic ROT-treatment decreased pH_{cyto} , pH_{mito} was unaffected, suggesting a lack of net proton accumulation into the mitochondrial matrix. In case of AA, both pH_{mito} and pH_{cyto} became more acidic. Semi-quantitative calculation of ΔpH revealed that this gradient was increased in ROT-treated and slightly decreased in AA-treated cells, suggesting that a difference in ΔpH might contribute to $\Delta\psi$ hyperpolarization and depolarization.

In healthy cells, net $\Delta\psi$ not only depends on ETC activity but also on forward- or reverse-mode action of CV and the ANT. For instance, we recently demonstrated that a greatly reduced CV expression and CV maximal activity was linked to $\Delta\psi$ hyperpolarization in fibroblasts of patients with TMEM70 mutations [14]. Qualitative experiments revealed that acute inhibition of CV using OLI does not induce $\Delta\psi$ depolarization in CT or ROT-treated cells. In contrast, acute CV inhibition rapidly depolarized $\Delta\psi$ in AA-treated cells. These data demonstrate that CV runs in reverse-mode in AA-treated cells whereas this is not the case in CT and ROT-treated cells. CV reverse-mode action in AA-treated cells likely is fuelled by ATP derived from mitochondrial substrate-level phosphorylation [3,43]. Our current results are supported by a previous study where we investigated immortalized embryonic fibroblasts of *NDUFS4*^{-/-} mice, a genetic model of CI deficiency [18]. In these cells we also observed that $\Delta\psi$ hyperpolarization in *NDUFS4*^{-/-} MEFs was

maintained in the absence of CV reverse-mode action. Acute ANT inhibition by BA did not induce $\Delta\psi$ depolarization in CT and ROT- or AA-treated cells, meaning that the ROT- and AA-induced effects on $\Delta\psi$ in these cells do not involve ANT reverse-mode action. We propose that the increased dependency of AA-treated cells on extracellular glucose to sustain their $[ATP]_c$ might reflect a lack of mitochondrial ATP production and transport to the cytosol. In this sense, ROT-treated cells appeared slightly less dependent on extracellular glucose, compatible with reduced activity of CV and the ANT.

5. Conclusions

Taken together, our results support a model (Fig. 6B), in which ROT-induced CI inhibition greatly reduces but not completely blocks cellular O_2 consumption. This residual O_2 consumption (CIV activity) is associated with substrate oxidation (CII activity) and proton efflux (CIII and CIV activity). ROT-treated cells displayed a very low residual O_2 consumption, $\Delta\psi$ hyperpolarization and an increased ΔpH . This strongly suggests that also CV and ANT activity (both running in forward mode) are greatly reduced. The latter effect might be enhanced by the drop in cytosolic pH, known to inhibit CV and ANT activity during lactate accumulation in glycolytic cells [3]. Both ROT- or AA-treated cells displayed a similarly reduced mitochondrial free ATP concentration ($[ATP]_m$). In ROT-treated cells, this drop likely results from reduced CV/ANT forward mode action. In case of AA-treatment the lower $[ATP]_m$ arises from CV reverse-mode action, the lack of ANT reverse mode action, and the inability of substrate level phosphorylation to meet the ATP demand of CV (Fig. 6C). We postulate that in ROT-treated cells $\Delta\psi$ hyperpolarization is the net result of: (i) a greatly reduced matrix proton efflux (CIII and CIV), (ii) a greatly reduced proton influx (*via* CV) (iii) a low-level ANT-mediated influx of positive charge, and (iv) an increase in ΔpH due to cytosolic acidification. The latter was also observed in AA-treated cells and likely results from upregulation of the glycolysis pathway [43].

Acknowledgements

This research was supported by a grant from the Netherlands Organisation for Scientific Research (NWO, No: 911-02-008), the Energy4All Foundation, and the NWO Centres for Systems Biology Research initiative (CSBR09/013V). M.R.W. and A.W. were supported by the grant from the Polish National Science Centre (UMO-2011/01/M/NZ3/02128). We thank Ing. H. Swarts (Dept. of Biochemistry 286) for generating the baculoviruses and Dr. H. Imamura (Kyoto University, Japan) for providing the ATeam and “dead-ATeam” vectors.

References

- [1] W.J.H. Koopman, P.H.G.M. Willems, J.A.M. Smeitink, Monogenic mitochondrial disorders, *N. Engl. J. Med.* 366 (2012) 1132–1141.
- [2] D.G. Nicholls, O. Lindberg, Inhibited respiration and ATPase activity of rat liver mitochondria under conditions of matrix condensation, *FEBS Lett.* 25 (1972) 61–64.
- [3] C. Chinopoulos, Mitochondrial consumption of cytosolic ATP: not so fast, *FEBS Lett.* 585 (2011) 1255–1259.
- [4] F. Palmieri, Diseases caused by defects of mitochondrial carriers: a review, *Biochim. Biophys. Acta* 1777 (2008) 564–578.
- [5] W.J.H. Koopman, L.G.J. Nijtmans, C.E.J. Dieteren, P. Roestenberg, F. Valsecchi, J.A.M. Smeitink, et al., Mammalian mitochondrial complex I: biogenesis, regulation, and reactive oxygen species generation, *Antioxid. Redox Signal.* 12 (2010) 1431–1470.
- [6] F. Fischer, A. Hamann, H.D. Osiewicz, Mitochondrial quality control: an integrated network of pathways, *Trends Biochem. Sci.* 37 (2012) 284–292.
- [7] J. Nunnari, A. Suomalainen, Mitochondria: in sickness and in health, *Cell* 148 (2012) 1145–1159.
- [8] E.I. Rugari, T. Langer, Mitochondrial quality control: a matter of life and death for neurons, *EMBO J.* 31 (2012) 1336–1349.
- [9] E.A. Schon, S. DiMauro, M. Hirano, Human mitochondrial DNA: roles of inherited and somatic mutations, *Nat. Rev. Genet.* 13 (2012) 878–890.
- [10] R.A.J. Smith, R.C. Hartley, H.M. Cochemé, M.P. Murphy, Mitochondrial pharmacology, *Trends Pharmacol. Sci.* 33 (2012) 341–352.
- [11] S.B. Vafai, V.K. Mootha, Mitochondrial disorders as windows into an ancient organelle, *Nature* 491 (2012) 374–383.

- [12] W.J.H. Koopman, F. Distelmaier, J.A.M. Smeitink, P.H.G.M. Willems, OXPHOS mutations and neurodegeneration, *EMBO J.* 32 (2013) 9–29.
- [13] G. Solaini, G. Sgarbi, G. Lenaz, A. Baracca, Evaluating mitochondrial membrane potential in cells, *Biosci. Rep.* 27 (2007) 11–21.
- [14] A.I. Jonckheere, M. Huigslot, M. Lammens, J. Jansen, L.P. van den Heuvel, U. Spiekerkoetter, et al., Restoration of complex V deficiency caused by a novel deletion in the human TMEM70 gene normalizes mitochondrial morphology, *Mitochondrion* 11 (2011) 954–963.
- [15] F. Distelmaier, H.-J. Visch, J.A.M. Smeitink, E. Mayatepek, W.J.H. Koopman, P.H.G.M. Willems, The antioxidant Trolox restores mitochondrial membrane potential and Ca^{2+} -stimulated ATP production in human complex I deficiency, *J. Mol. Med.* 87 (2009) 515–522.
- [16] F. Distelmaier, W.J.H. Koopman, L.P. van den Heuvel, R.J. Rodenburg, E. Mayatepek, P.H.G.M. Willems, et al., Mitochondrial complex I deficiency: from organelle dysfunction to clinical disease, *Brain* 132 (2009) 833–842.
- [17] W.J.H. Koopman, S. Verkaart, H.-J. Visch, F.H. van der Westhuizen, M.P. Murphy, L.W. P.J. van den Heuvel, et al., Inhibition of complex I of the electron transport chain causes O_2^- -mediated mitochondrial outgrowth, *Am. J. Physiol. Cell Physiol.* 288 (2005) C1440–C1450.
- [18] F. Valsecchi, C. Monge, M. Forkink, A.J.C. de Groof, G. Benard, R. Rossignol, et al., Metabolic consequences of NDUF54 gene deletion in immortalized mouse embryonic fibroblasts, *Biochim. Biophys. Acta* 1817 (2012) 1925–1936.
- [19] A.Y. Abramov, T.K. Smulders-Srinivasan, D.M. Kirby, R. Acin-Perez, J.A. Enriquez, R.N. Lightowlers, et al., Mechanism of neurodegeneration of neurons with mitochondrial DNA mutations, *Brain* 133 (2010) 797–807.
- [20] A. Barrientos, C.T. Moraes, Titrating the effects of mitochondrial complex I impairment in the cell physiology, *J. Biol. Chem.* 274 (1999) 16188–16197.
- [21] A. Mehta, C. Shaha, Apoptotic death in *Leishmania donovani* promastigotes in response to respiratory chain inhibition: complex II inhibition results in increased pentamidine cytotoxicity, *J. Biol. Chem.* 279 (2004) 11798–11813.
- [22] Q. Gao, M.S. Wolin, Effects of hypoxia on relationships between cytosolic and mitochondrial NAD(P)H redox and superoxide generation in coronary arterial smooth muscle, *Am. J. Physiol. Heart Circ. Physiol.* 295 (2008) H978–H989.
- [23] B.J. Van Raam, W. Sluiter, E. De Wit, D. Roos, A.J. Verhoeven, T.W. Kuijpers, Mitochondrial membrane potential in human neutrophils is maintained by complex III activity in the absence of supercomplex organisation, *PLoS One* 3 (2008) 12.
- [24] C.E.J. Dieteren, P.H.G.M. Willems, R.O. Vogel, H.G. Swarts, J. Fransen, R. Roepman, et al., Subunits of mitochondrial complex I exist as part of matrix- and membrane-associated subcomplexes in living cells, *J. Biol. Chem.* 283 (2008) 34753–34761.
- [25] C.E.J. Dieteren, S.C.A.M. Gielen, L.G.J. Nijtmans, J.A.M. Smeitink, H.G. Swarts, R. Brock, et al., Solute diffusion is hindered in the mitochondrial matrix, *Proc. Natl. Acad. Sci. U. S. A.* 108 (2011) 8657–8662.
- [26] C.E.J. Dieteren, W.J.H. Koopman, H.G. Swarts, J.G.P. Peters, P. Maczuga, J.J. van Gemst, et al., Subunit-specific incorporation efficiency and kinetics in mitochondrial complex I homeostasis, *J. Biol. Chem.* 287 (2012) 41851–41860.
- [27] S.J.G. Hoefs, C.E.J. Dieteren, F. Distelmaier, R.J.R.J. Janssen, A. Epplen, H.G.P. Swarts, et al., NDUF2 complex I mutation leads to Leigh disease, *Am. J. Hum. Genet.* 82 (2008) 1306–1315.
- [28] D. Poburko, J. Santo-Domingo, N. Demareux, Dynamic regulation of the mitochondrial proton gradient during cytosolic calcium elevations, *J. Biol. Chem.* 286 (2011) 11672–11684.
- [29] H. Imamura, K.P.H. Nhat, H. Togawa, K. Saito, R. Iino, Y. Kato-Yamada, et al., Visualization of ATP levels inside single living cells with fluorescence resonance energy transfer-based genetically encoded indicators, *Proc. Natl. Acad. Sci. U. S. A.* 106 (2009) 15651–15656.
- [30] E. Hütter, H. Unterluggauer, A. Garedew, P. Jansen-Dürr, E. Gnaiger, High-resolution respirometry—a modern tool in aging research, *Exp. Gerontol.* 41 (2006) 103–109.
- [31] E. Gnaiger, A. Kuznetsov, S. Schneeberger, R. Seiler, G. Brandacher, W. Steurer, et al., Mitochondria in the cold, in: G. Heldmaier, M. Klingenspor (Eds.), *Life Cold*, Springer, Heidelberg, Berlin, New York, 2000, pp. 431–438.
- [32] M. Nooteboom, M. Forkink, P.H.G.M. Willems, W.J.H. Koopman, Live-cell quantification of mitochondrial functional parameters, in: E. Badoer (Ed.), *Neuromethods Vis. Tech.—From Immunohistochem. to Magn. Reson. Imaging*, Humana Press Inc., 2012, pp. 111–127.
- [33] J.S. Fan, P. Palade, Perforated patch recording with beta-escin, *Pflügers Arch.* 436 (1998) 1021–1023.
- [34] W.J.H. Koopman, H.-J. Visch, S. Verkaart, L.W.P.J. van den Heuvel, J.A.M. Smeitink, P.H.G.M. Willems, Mitochondrial network complexity and pathological decrease in complex I activity are tightly correlated in isolated human complex I deficiency, *Am. J. Physiol. Cell Physiol.* 289 (2005) C881–C890.
- [35] P. Srivastava, D. Panda, Rotenone inhibits mammalian cell proliferation by inhibiting microtubule assembly through tubulin binding, *FEBS J.* 274 (2007) 4788–4801.
- [36] E.N. Maldonado, J. Patnaik, M.R. Mullins, J.J. Lemasters, Free tubulin modulates mitochondrial membrane potential in cancer cells, *Cancer Res.* 70 (2010) 10192–10201.
- [37] A.V. Kuznetsov, S. Javadov, R. Guzun, M. Grimm, V. Saks, Cytoskeleton and regulation of mitochondrial function: the role of beta-tubulin II, *Front. Physiol.* 4 (2013) 82.
- [38] J.G. Okun, P. Lümmer, U. Brandt, Three classes of inhibitors share a common binding domain in mitochondrial complex I (NADH:ubiquinone oxidoreductase), *J. Biol. Chem.* 274 (1999) 2625–2630.
- [39] D.G. Nicholls, Simultaneous monitoring of ionophore- and inhibitor-mediated plasma and mitochondrial membrane potential changes in cultured neurons, *J. Biol. Chem.* 281 (2006) 14864–14874.
- [40] D.G. Nicholls, S.J. Ferguson, 3rd ed., *Bioenergetics*, 3, Academic Press, London, 2002.
- [41] I. Goehring, A.A. Gerencser, S. Schmidt, M.D. Brand, H. Mulder, D.G. Nicholls, Plasma membrane potential oscillations in insulin secreting Ins-1 832/13 cells do not require glycolysis and are not initiated by fluctuations in mitochondrial bioenergetics, *J. Biol. Chem.* 287 (2012) 15706–15717.
- [42] G. Cannino, R. El-Khoury, M. Pirinen, B. Hutz, P. Rustin, H.T. Jacobs, et al., Glucose modulates respiratory complex I activity in response to acute mitochondrial dysfunction, *J. Biol. Chem.* 287 (2012) 38729–38740.
- [43] C. Chinopoulos, A.A. Gerencser, M. Mandi, K. Mathe, B. Töröcsik, J. Doczi, et al., Forward operation of adenine nucleotide translocase during F₀F₁-ATPase reversal: critical role of matrix substrate-level phosphorylation, *FASEB J.* 24 (2010) 2405–2416.